Whitmarsh, R.B., Sawyer, D.S., Klaus, A., and Masson, D.G. (Eds.), 1996
Proceedings of the Ocean Drilling Program, Scientific Results, Vol. 149

49. *DATA REPORT:* TEXTURAL AND MINERAL COMPOSITION OF CENOZOIC SEDIMENTARY FACIES OFF THE WESTERN IBERIAN PENINSULA, SITES 897, 898, 899, and 900[1]

B. Alonso,[2] M.C. Comas,[3] G. Ercilla,[2] and A. Palanques[2]

ABSTRACT

Textural parameters, granulometric statistical parameters (mean, standard deviation, skewness, and kurtosis), cumulative curve shape of grain-size distribution, sand fraction composition, carbonate content, and bulk mineralogy were determined for Cenozoic sediments of lithostratigraphic Units I and II recovered at Sites 897, 898, 899, and 900 on Ocean Drilling Program Leg 149. These data allow us to discriminate among and characterize the three main sedimentary facies (pelagic/hemipelagic, turbidite, and contourite) recognized in the Cenozoic (Pleistocene to Eocene) deposits of the Iberia Abyssal Plain. This report describes the textural analysis and mineral composition for these three sedimentary facies.

INTRODUCTION

On Ocean Drilling Program (ODP) Leg 149, in the southern part of the Iberia Abyssal Plain, the ocean/continent transition of the rifted continental margin off west Iberia was drilled along a 40° to 41°N latitude transect at Sites 897, 898, 899, 900, and 901 (Fig. 1). Cenozoic Paleocene to Pleistocene postrift sediments (up to 750 m thick) were recovered at four sites (897, 898, 899, and 900).

Site 897 (5386 m water depth) is the farthest from the continental margin off Portugal. This site is located over a north-south-trending basement ridge of serpentinized peridotites within the ocean/continent transition. The sedimentary section (Holes 897A, 897C, and 897D) includes about 700 m of Pleistocene to Lower Cretaceous deposits. Four lithostratigraphic units were identified (Shipboard Scientific Party, 1994). We analyzed sediments from Unit I and Unit II. Unit I (0-292.0 m below seafloor [mbsf]) is Pleistocene and early Pliocene in age. Unit II (292.0-619.7 mbsf) corresponds to lower Miocene to middle Eocene sediments and was divided into three subunits (IIA, IIB, and IIC).

Site 898 (main Hole 898A, 5279 m water depth) is located over a semielliptical basement ridge, also within the presumed ocean/continent transition zone (Shipboard Scientific Party, 1994). Two lithostratigraphic units were identified (Shipboard Scientific Party, 1994), and sediments from both units were analyzed. Unit I (0-163.4 mbsf) has a Pleistocene to late Pliocene age. Unit II was subdivided into Subunit IIA (163.4-172.2 mbsf), which is middle Miocene in age, and Subunit IIB (172.2-339.7 mbsf) consists of sediments from the middle Miocene to upper Oligocene.

Site 899 (Holes 899A and 899B, 5291 m water depth) is located over a semielliptical basement ridge. The four lithostratigraphic units identified at Site 899 include about 550 m of Pleistocene to Cretaceous deposits (Shipboard Scientific Party, 1994). We analyzed sediments from Unit I and Unit II. Unit I (81.50-131.65 mbsf, Hole 899A) is of Pliocene age. In Unit II, two Subunits were identified as Subunit IIA (131.65-206.6 mbsf, Hole 899B), which is early Pliocene to middle Miocene in age, and Subunit IIB (206.6-228.6 mbsf in Hole 899A and 230.5-360.2 in Hole 899B), which is Miocene to Oligocene in age.

Site 900 (main Hole 900A, 5037 m water depth) is located near the transition between the continental rise and abyssal plain, and it is closer to Porto Seamount and the mouth of the Nazaré Canyon than the other sites (Fig. 1). This site was drilled over an angular basement high that appears to be a tilted fault block. Two lithostratigraphic units were identified at Site 900 (Shipboard Scientific Party, 1994). Three Subunits were identified within Unit I: Subunit IA (0-67.2 mbsf) is Pleistocene to late Pliocene in age, Subunit IB (67.2-96.0 mbsf) is late Pliocene to late Miocene in age, and Subunit IC (96.0-181.5 mbsf) is late Miocene to late early Miocene in age. Two subunits were identified within Unit II. Subunit IIA (181.5-234.3 mbsf) is early Miocene in age, and Subunit IIB (234.3-748-9 mbsf) is early Miocene to Paleocene in age. We analyzed samples from Subunits IA, IB, IC, IIA, and IIB, ranging in age from Pleistocene to early Miocene.

This paper reports the textural and mineralogical data from selected sediment samples from these four sites. Our data presentation focuses on describing and typifying the major Cenozoic sedimentary facies recovered on Leg 149 on the basis of textural parameters and bulk mineralogy.

METHODS

Textural Analysis

Textural analyses were performed using settling-tube techniques for the coarse-grained fraction (>50 µm) and Sedigraph 5000 D techniques for the silt and clay fractions (<50 µm) (Giró and Maldonado, 1985). Grain-size distributions were plotted in a cumulative curve and frequency histogram for each sample. Textural statistical parameters (mean, standard deviation, skewness, and kurtosis) were calculated using moment measurements on sample populations containing quarter-phi interval classes in all fractions (Friedman and Sanders, 1978; Forrest and Clark, 1989). The following ranges of standard deviation were adopted for the classification of sediment into sorting classes (Friedman and Sanders, 1978; Alonso and Maldonado, 1990; Ercilla et al., 1994):

moderately well sorted sediments: 0.50ϕ to 0.80 ϕ,
moderately sorted sediments: 0.80 ϕ to 1.40 ϕ,
poorly sorted sediments: 1.40 ϕ to 2.00 ϕ,
very poorly sorted sediments: 2.00 ϕ to 2.60 ϕ.

[1]Whitmarsh, R.B., Sawyer, D.S., Klaus, A., and Masson, D.G. (Eds.), 1996. *Proc. ODP, Sci. Results,* 149: College Station, TX (Ocean Drilling Program).
[2]Instituto de Ciencias del Mar, CSIC, Paseo Joan de Borbó s/n, 08039 Barcelona, Spain. belen@masagran.icm.csic.es
[3]Instituto Andaluz de Geología Mediterranea, CSIC, Universidad de Granada, Campus Universitario, 18071 Granada, Spain.

The fine-grained fraction (pelite fraction, <50 µm) was plotted in cumulative curves to identify sediment types according to hydrodynamic depositional processes (Gonthier et al., 1981). Three different cumulative curve shapes were identified by the slope gradient according to Riviere (1977): (1) hyperbolic (0°-15°), (2) logarithmic (15°-45°), and (3) parabolic (>45°). These curve shapes correspond the granulometric facies and sedimentary processes described by Riviere (1977) and Gonthier et al. (1981). The hyperbolic curves are observed in pelagic/hemipelagic deposits. Logarithmic curves tending toward hyperbolic represent turbiditic/contouritic silty clays, whereas those tending toward parabolic correspond to turbiditic/contouritic silts and sandy silts. The parabolic curves occur in turbiditic/contouritic coarse-grained deposits (sand and silt).

The nature of the pelite fraction (<50 µm) was examined with a Hitachi S-750 scanning electron microscope (SEM). These data were included within the sedimentological data set to define the sedimentary facies.

Sand fraction (>63 µm) composition was studied using a binocular microscope. Abundances of different components were estimated by counting about 300 grains per sample. The following components were identified and counted: light minerals (quartz, mica, feldspar, and others), heavy minerals, rock fragments, neoformation minerals (pyrite and pyritized tests and burrows, glauconite), bioclasts (pelagic foraminifers, benthic foraminifers, siliceous biogenic materials, pteropods), and others that include unidentifiable remains. For sand fraction components, the ranges used to describe the nature of the sediments are as follows:

biogenous sediments: >60% biogenous components,
mixed sediments: from 40% to 60% biogenous and terrigenous components,
terrigenous sediments: >60% terrigenous components.

Mineral Analysis

For the quantitative mineral analysis of marine sediments, which are multiphase mixtures, pure standards are not available to obtain calibration constants. Thus, standardless methods of quantitative X-ray analysis must be used. Many authors have developed complicated methods, from a practical point of view. To obviate the major problems of these methods, Rius et al. (1989) developed a simple standardless method that directly determines calibration constants using only diffracted intensities and calculated phase-absorption coefficients through a least-squares procedure. The relative abundances of illite, kaolinite, chlorite, quartz, calcite, dolomite, feldspar, and plagioclase were estimated following a method according to Rius et al. (1989), which has been used to analyze marine sediments (Palanques et al., 1990).

For the analysis of mineral phases, sediment samples were ground for 20 min in an agate mill and packed into sample holders. X-ray diffractograms were taken on a Siemens d-500 X-ray diffractometer. Cu Kα radiation, generated at 40 kV and 20 mA, a graphite monochromator, and a scintillation counter were used. Peaks were scanned from a 2θ of 4° to 50°, with a step-scan range of 1.2 θ-2 θ, an angular increment of 0.05/2 θ, and a counting time of 3 s/step. Diffractograms were visually interpreted with the help of a computerized search-and-match routine using Joint Committee on Powder Diffraction Standards files.

The carbonate content of the samples was determined using a Bernard calcimeter, according to the method described by Vatan (1967). This method measures the pressure of the CO_2 released when the sample is attacked with dilute HCl at atmospheric pressure. The bulk sample was previously pulverized to achieve total homogenization. Carbonate contents are expressed as weight percent $CaCO_3$, assuming that all carbonate was present as pure calcite (Table 1).

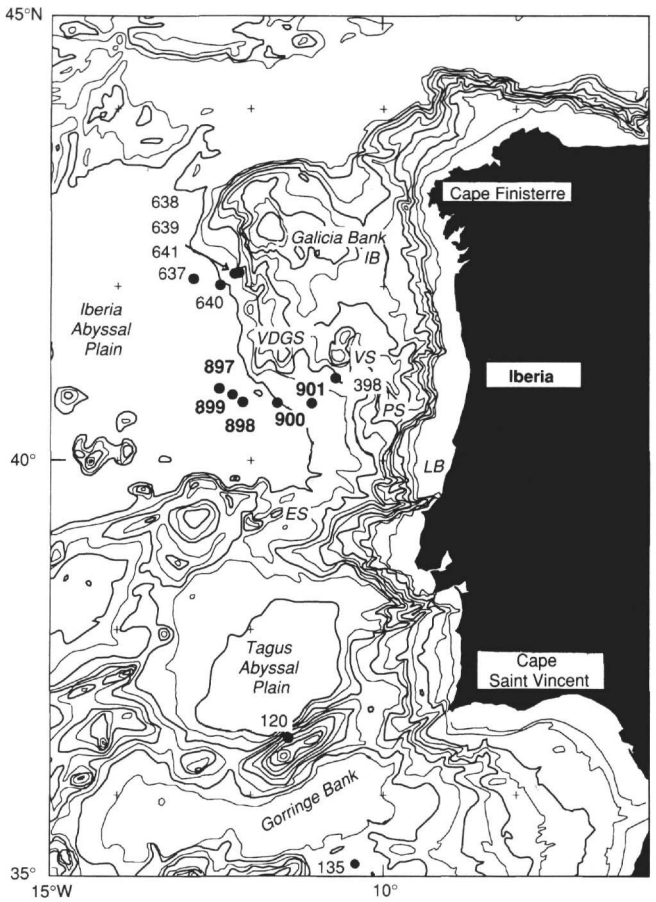

Figure 1. Bathymetric map showing the location of Sites 897, 898, 899, 900, and 901 from Leg 149, Site 398 from DSDP Leg 47, and Sites 637, 638, 639, 640, and 641 from ODP Leg 103.

RESULTS

Textural Analysis

The textural data consist of a total of 172 samples described in detail: 47 samples from Site 897, 44 samples from Site 898, 47 samples from Site 899, and 34 samples from Site 900. These samples were selected during post-cruise studies on recovered sediments and were available for shipboard sampling based on their relative abundance in the cores and as representative of all the sedimentary facies described on the core barrel sheets on board *JOIDES Resolution.*

The results of the textural analysis of selected samples of lithostratigraphic Units I and II from Sites 897, 898, 899, and 900 are shown in Table 1. The binary plots in Figures 2 and 3 show the relationship of standard deviation vs. mean particle size and kurtosis vs. skewness. On these plots, all samples analyzed from lithostratigraphic Units I and II are represented. The diagrams are indicators of the hydraulic regime on the Iberia Abyssal Plain during the Cenozoic. According to Sly et al. (1983), these data indicate that Cenozoic sediments in the Iberia Abyssal Plain were deposited under low-energy conditions.

Sedimentological data such as texture, grain-size statistics, cumulative shape curves of the grain-size distribution, and sand fraction composition allow us to characterize the different Cenozoic sedimentary facies recovered on Leg 149 (Palanques and Maldonado, 1985; Comas and Maldonado, 1988; Alonso and Maldonado, 1990; Ercilla et al., 1994). Grain-size analysis of the sediments was oriented to-

Table 1. Textural data from recovered Cenozoic sediments (Holes 897A, 897C, 898A, 898B, 899A, 899B, and 900A).

Core, section, interval (cm)	$CaCO_3$ (%)	Sand (%)	Silt (%)	Clay (%)	Mean grain size (ø)	Deviation (ø)	Skewness (ø)	Kurtosis (ø)	Lithostratigraphic unit	Age
149-897A-										
1R-1, 25-27	7	96.00	4.00	0.00	1.43	0.68	1.81	6.04	Unit I: silty clayey to clayey silt, nannofossil clay	Pleistocene
1R-1, 63-65	10	5.11	62.20	32.69	6.91	2.08	−0.16	3.73		Pleistocene
3R-CC, 8-10	15	5.80	43.57	50.62	7.76	2.03	−0.78	4.14		Pleistocene
4R-3, 115-117	43	10.49	20.25	69.25	8.49	2.50	−0.89	3.21		Pleistocene
5R-2, 127-129	22	1.86	35.11	63.03	8.55	1.89	−0.32	3.41		Pleistocene
8R-5, 16-18	18	0.40	32.30	67.26	8.68	1.71	0.02	2.86		Pleistocene
149-897C-										
2R-1, 65-67	6	0.01	45.04	54.96	8.32	1.71	0.37	2.23		Pleistocene
2R-CC, 3-5	18	50.26	20.69	29.05	5.67	2.96	0.62	1.89		Pleistocene
3R-1, 18-20	24	48.26	18.14	33.59	5.49	3.52	0.23	1.62		Pleistocene
5R-1, 85-87	29	0.01	30.53	69.47	8.67	1.32	0.24	2.51		Pleistocene
8R-3, 97-99	14	2.95	54.28	42.77	7.56	1.75	−0.15	2.79		late Pliocene
8R-3, 104-106	10	26.74	50.90	22.36	5.93	2.50	0.42	2.61		late Pliocene
9R-1, 86-88	12	1.92	54.06	44.02	7.62	1.79	0.18	2.30		late Pliocene
10R-1, 88-90	19	29.38	49.72	20.90	5.76	2.18	0.38	2.27		late Pliocene
14R-2, 32-34	26	1.60	51.90	46.50	7.68	1.64	0.16	2.96		late Pliocene
15R-3, 22-24	38	4.31	40.93	54.76	8.00	1.91	−0.36	3.25		early/late Pliocene
15R-3, 31-33	14	0.01	49.75	50.25	8.14	1.66	0.47	2.42		early/late Pliocene
16R-2, 37-39	10	18.01	66.49	15.50	5.94	1.84	0.60	2.95		early/late Pliocene
17R-2, 21-23	65	1.24	29.00	69.76	8.86	1.82	−0.27	2.92		early/late Pliocene
19R-3, 24-26	16	2.33	53.58	44.04	7.75	1.83	−0.15	3.84		early Pliocene
19R-3, 38-40	7	32.99	52.42	14.58	5.52	2.07	0.65	2.97		early Pliocene
20R-2, 19-21	41	0.01	39.61	60.39	8.50	1.66	0.17	2.26		early Pliocene
20R-2, 74-76	20	0.01	42.56	57.44	8.28	1.60	0.36	2.50		early Pliocene
20R-2, 96-98	10	0.44	55.40	44.17	7.86	1.67	0.40	2.63		early Pliocene
22R-2, 1-3	7	3.89	43.69	52.43	8.00	2.10	−0.38	3.93		early Pliocene
23R-1, 22-24	8	0.01	48.37	51.63	8.01	1.74	0.63	2.65		early Pliocene
23R-1, 28-30	12	1.67	52.52	45.81	7.79	1.75	0.01	2.61		
26R-2, 29-31	19	1.01	28.78	70.20	8.67	1.79	−0.08	2.64	Subunit IIA: nannofossil claystone, claystone	early Pliocene
28R-3, 3-5	8	1.93	43.34	54.72	8.28	2.09	−0.01	2.27	Subunit IIB: calcareous claystone, claystone	Miocene
30R-4 40-42	47	13.87	52.92	33.21	6.88	2.24	0.3	42.30		Miocene
40R-6, 71-74	31	23.90	58.55	17.55	5.98	2.01	0.5	62.61	Subunit IIC: silty claystone to clayey siltstone, calcareous siltstone	Oligocene
47R-1, 61-63	11	9.42	44.77	45.81	7.53	2.33	0.20	2.22		Oligocene
49R-2, 37-39	17	2.74	58.89	38.37	7.46	1.94	0.51	2.69		Oligocene
49R-3, 49-51	5	0.01	30.82	69.18	8.67	1.67	0.56	2.44		Oligocene
49R-4, 13-15	33	0.01	45.06	54.94	8.20	1.57	0.53	2.93		Oligocene
50R-1, 49-51	5	0.01	40.28	59.72	8.51	1.78	0.39	2.23		Eocene
50R-1, 143-145	40	7.44	61.62	30.94	6.99	1.98	0.04	3.54		Eocene
50R-2, 130-132	40	3.02	56.83	40.15	7.49	1.82	0.22	2.80		Eocene
50R-3, 9-11	25	1.53	54.82	43.65	7.66	1.75	0.19	2.27		Eocene
51R-2, 47-49	40	1.87	57.32	40.81	7.56	1.53	0.07	2.68		Eocene
51R-2, 55-57	4	0.01	36.69	63.31	8.52	1.73	0.39	2.19		Eocene
51R-3, 111-113	33	0.01	48.87	51.13	7.99	1.30	0.60	2.78		Eocene
52R-2, 29-31	39	0.01	61.07	38.93	7.72	1.45	0.59	3.19		Eocene
54R-4, 7-9	47	0.01	50.74	49.26	7.76	1.21	0.35	2.96		Eocene
55R-1, 115-117	27	3.46	67.88	28.66	7.08	1.67	0.42	2.66		Eocene
55R-2, 81-83	7	0.01	32.89	67.11	8.89	1.68	0.21	2.14		Eocene
56R-5, 57-59	4	1.61	51.58	46.80	7.71	2.07	−0.46	5.41		Eocene
149-898A-										
1H-1, 3-5	17	15.00	45.70	39.10	7.12	2.37	−0.24	2.46	Unit I: silty clay to clayey silt, silt, and fine sand	Pleistocene
1H-3, 144-146	14	2.50	32.07	65.40	8.52	1.80	−0.20	3.81		Pleistocene
1H-5, 128-130	29	72.64	18.41	8.94	4.16	2.12	1.44	4.09		Pleistocene
1H-5, 145-147	20	6.40	29.13	64.47	8.17	2.06	−0.41	2.91		Pleistocene
2H-5, 139-141	8	58.66	38.24	3.10	4.27	1.40	1.49	4.99		Pleistocene
2H-5, 144-146	39	2.37	28.74	68.90	8.60	1.87	−0.39	3.12		Pleistocene
3H-4, 7-9	82	4.17	14.30	81.54	8.86	1.70	−1.61	6.20		Pleistocene
3H-4, 53-55	9	59.59	36.44	3.96	4.29	1.50	1.48	5.35		Pleistocene
4H-6, 141-143	10	15.02	71.11	13.88	5.87	1.76	0.40	3.44		Pleistocene
5H-3, 59-61	7	71.01	22.02	6.97	4.36	1.84	1.64	4.81		Pleistocene
5H-4, 9-11	8	1.75	46.41	51.84	8.07	1.70	0.20	3.06		Pleistocene
5H-6, 35-37	5	0.01	41.08	58.92	8.46	1.62	0.34	2.35		Pleistocene
8H-2, 120-122	8	82.54	14.44	3.02	3.81	1.47	2.32	9.64		Pleistocene
8H-4, 38-40	5	12.19	40.60	47.21	7.58	2.47	−0.42	2.60		Pleistocene
9H-4, 42-45	17	58.86	31.18	9.96	4.68	2.03	0.95	3.13		Pleistocene
9H-7, 19-22	18	0.01	55.57	44.43	7.87	1.70	0.51	2.31		Pleistocene
10H-4, 110-112	30	2.25	26.73	71.01	8.53	1.63	−0.9	54.12		Pleistocene
10H-6, 95-97	6	83.26	12.26	4.48	3.49	1.76	1.86	7.41		Pleistocene
12H-6, 130-132	10	43.52	43.95	12.53	5.10	2.14	0.64	2.87		Pleistocene
13H-4, 32-34	53	3.49	25.42	71.08	8.50	1.94	−0.4	84.02		Pleistocene
15X-2, 98-100	13	0.01	58.98	41.02	7.59	1.42	0.52	2.38		Pleistocene
15X-2, 115-117	52	6.74	48.47	44.79	7.56	2.23	0.09	2.67		Pleistocene
16X-2, 95-97	13	59.79	26.73	13.48	4.61	2.49	0.74	2.96		Pleistocene
17X-3, 11-12	46	4.50	32.97	62.53	8.30	1.87	−0.6	63.96		Pliocene
17X-5, 16-18	16	55.92	31.02	13.06	4.81	2.27	0.80	3.20		Pliocene
18X-4, 97-100	6	2.20	26.13	71.67	8.75	1.78	−0.54	3.81	Subunit IIA: silty clay to clayey silt, nannofossil clay	middle Miocene
18X-6, 129-132	4	0.01	46.66	53.34	8.36	1.96	0.31	2.08		middle Miocene
18X-CC, 1-4	50	1.42	32.46	66.13	8.51	1.67	−0.44	3.47		middle Miocene
19X-1, 64-66	14	1.02	36.10	62.88	8.43	1.89	0.13	2.51		middle Miocene
19X-2, 21-23	49	0.20	36.83	62.88	8.36	1.68	−0.03	2.59	Subunit IIB: silty claystone to clayey siltstone, nannofossil claystone	middle Miocene

Table 1 (continued).

Core, section, interval (cm)	$CaCO_3$ (%)	Sand (%)	Silt (%)	Clay (%)	Mean grain size (ø)	Deviation (ø)	Skewness (ø)	Kurtosis (ø)	Lithostratigraphic unit	Age
19X-6, 84-86	24	15.12	53.10	31.78	6.80	2.17	0.28	2.14		middle Miocene
19X-CC, 18-20	42	13.37	50.34	36.29	6.93	2.20	0.11	2.06		middle Miocene
20X-4, 144-146	38	25.73	52.86	21.41	6.01	2.27	0.33	2.64		middle Miocene
21X-2, 96-98	17	5.13	37.75	57.12	7.99	2.00	−0.23	2.66		middle Miocene
22X-1, 130-132	33	13.17	43.95	42.88	7.31	2.27	0.02	2.09		middle Miocene
27X-3, 38-40	22	23.52	56.19	20.29	6.14	2.21	0.81	2.89		early Miocene
27X-5, 136-138	20	21.69	64.93	13.39	5.69	1.84	0.78	3.33		early Miocene
28X-4, 106-108	14	52.92	31.10	15.98	5.12	2.50	1.08	3.12		early Miocene
29X-3, 12-14	16	18.32	50.01	31.67	6.46	2.31	0.17	2.42		early Miocene
29X-4, 136-138	8	3.48	36.64	59.88	8.48	2.04	−0.38	3.37		early Miocene
30X-3, 131-33	15	18.08	65.01	16.91	6.41	1.94	0.40	3.32		late Oligocene
33X-2, 143-145	16	29.62	47.74	22.67	6.08	2.35	0.56	2.45		late Oligocene
149-898B-										
1H-1, 41-43	25	21.34	35.99	42.66	7.10	2.58	−0.14	1.91	Subunit IIB	late Oligocene
1H-2, 127-129	10	57.88	21.99	20.13	5.10	2.68	0.88	2.41		late Oligocene
149-899A-										
1R-3, 33-35	18	2.90	43.82	53.28	7.97	1.78	−0.27	2.87	Unit I: silty clay to clayey silt, nannofossil clay	late Pliocene
1R-3, 68-70	17	31.89	40.01	28.11	6.23	2.50	0.34	1.91		late Pliocene
1R-3, 125-127	33	42.49	32.40	25.13	5.78	2.62	0.37	1.90		late Pliocene
4R-1, 43-45	64	3.64	30.45	65.91	8.30	1.78	−0.48	3.72		early/late Pliocene
4R-2, 28-30	11	0.01	50.64	49.36	8.03	1.54	0.43	2.45		early/late Pliocene
4R-2, 34-36	8	34.91	52.21	12.91	5.44	2.08	0.99	3.56		early/late Pliocene
5R-3, 42-44	29	1.20	49.72	49.07	7.85	1.68	−0.15	3.78		early/late Pliocene
5R-3, 100-102	61	4.87	29.64	65.49	8.30	2.03	−0.54	3.71		early/late Pliocene
5R-3, 103-105	43	46.40	43.86	9.74	5.04	1.85	0.88	2.75		early/late Pliocene
6R-1, 125-127	23	20.21	33.39	46.41	6.96	2.73	−0.33	2.37	Subunit IIA: calcareous claystone, nannofossil claystone	late Miocene
6R-2, 100-102	36	41.00	29.36	29.60	6.00	2.70	0.49	1.85		late Miocene
6R-3, 112-114	30	4.27	25.61	66.77	8.19	2.77	−1.96	7.62		late Miocene
8R-1, 20-22	50	0.01	26.88	73.12	8.50	1.32	0.45	2.65		late Miocene
8R-1, 81-83	30	16.63	33.20	50.10	7.10	2.57	−0.49	2.38		late Miocene
8R-1, 100-102	42	6.24	42.17	51.59	7.60	1.97	−0.12	2.39		late Miocene
8R-1, 112-114	33	3.52	32.22	64.26	8.54	1.80	−0.77	4.36		late Miocene
9R-1, 67-69	14	41.71	28.97	29.31	6.00	2.85	0.55	1.95		late Miocene
9R-2, 110-112	4	3.67	44.94	51.39	8.03	2.04	−0.02	2.20		middle/late Miocene
11R-1, 91-93	45	1.10	33.13	65.77	8.50	1.55	−0.08	3.64		middle/late Miocene
11R-1, 129-131	13	0.40	34.33	65.27	8.71	1.91	−0.08	2.24		middle/late Miocene
14R-2, 7-9	5	8.67	37.78	53.50	7.93	2.36	−0.15	2.25	Subunit IIB: silty claystone to clayey siltstone, nannofossil siltstone	early/middle Miocene
14R-2, 29-31	43	29.02	60.31	10.67	5.20	1.74	1.41	4.51		early/middle Miocene
14R-2, 108-110	35	18.96	53.93	27.11	6.31	2.88	0.41	2.13		early/middle Miocene
14R-3, 62-64	50	47.90	36.00	13.88	5.10	2.06	1.10	3.07		early/middle Miocene
15R-5, 44-47	13	0.76	37.14	62.10	8.50	1.79	−0.15	2.57		early/middle Miocene
15R-5, 54-57	28	0.66	35.30	64.04	8.57	1.70	0.08	2.53		early/middle Miocene
15R-5, 58-61	37	9.90	56.17	33.80	6.89	1.87	0.10	2.28		early/middle Miocene
16R-1, 55-58	6	0.75	38.27	60.98	8.49	1.78	0.25	2.52		early/middle Miocene
16R-1, 108-111	5	3.40	40.50	56.10	8.26	2.11	−0.14	2.67		early/middle Miocene
16R-2, 15-18	6	3.20	41.28	55.52	8.11	2.12	−0.13	2.84		early/middle Miocene
149-899B-										
3R-1, 62-64	26	0.72	41.39	57.88	8.30	1.85	0.23	2.49		early Miocene
3R-1, 78-80	28	5.07	51.51	43.41	7.45	1.89	−0.39	3.06		early Miocene
5R-3, 135-137	38	5.88	39.58	54.53	8.05	1.92	−0.91	5.10		early Miocene
5R-5, 81-83	30	3.09	53.48	43.42	7.47	1.83	0.10	2.38		early Miocene
5R-6, 42-44	19	1.11	35.75	63.14	8.35	1.50	−0.11	3.51		early Miocene
6R-3, 98-100	10	0.01	43.08	56.91	8.30	1.61	0.39	2.34		early Miocene
6R-3, 104-106	26	39.62	35.11	25.27	5.86	2.50	0.51	1.98		early Miocene
8R-6, 84-86	5	0.96	48.55	50.48	7.90	1.67	0.33	2.54		Oligocene
9R-2, 86-88	22	12.33	58.04	29.63	6.63	2.03	0.29	2.22		Oligocene
10R-2, 128-130	6	0.01	46.91	53.08	8.19	1.63	0.35	2.30		Oligocene
11R-5, 45-47	4	0.01	46.28	53.71	8.19	1.59	0.38	2.29		Oligocene
12R-1, 111-113	5	0.01	48.48	51.51	8.15	1.83	0.48	2.34		Oligocene
12R-4, 132-134	4	0.83	48.65	50.52	8.09	1.85	0.44	2.47		Oligocene
12R-5, 10-12	17	0.01	47.95	52.04	7.93	1.44	0.06	2.34		Oligocene
13R-2, 40-42	4	0.01	53.98	46.01	7.90	1.72	0.57	2.36		Oligocene
13R-6, 70-72	3	0.62	42.76	56.61	8.40	1.85	0.13	2.33		Oligocene
14R-4, 56-58	11	0.01	40.28	59.72	8.34	1.44	0.64	2.85		Oligocene
149-900A-										
4R-1, 24-27	4	2.66	37.36	59.98	8.47	2.00	2.00	3.10	Subunit IA: nannofossil clay, clay, nannofossil ooze	Pleistocene
4R-1, 36-38	8	0.44	37.79	63.78	8.46	1.67	0.01	2.55		Pleistocene
4R-1, 44-47	65	2.02	27.28	70.70	8.34	1.62	−0.23	3.85		Pleistocene
5R-5, 35-37	41	2.59	35.22	62.19	8.28	1.79	−0.30	3.17		Pleistocene
5R-5, 55-57	15	2.83	44.09	53.07	8.00	1.79	−0.10	2.92		Pleistocene
5R-5, 66-68	6	6.75	67.04	26.21	6.95	1.96	0.51	2.91		Pleistocene
6R-6, 80-82	58	1.42	26.48	72.10	8.74	1.73	−0.39	3.30		Pleistocene
6R-6, 90-92	26	1.23	39.55	59.22	8.32	1.84	−0.02	2.38		Pleistocene
6R-6, 96-98	5	3.64	46.17	50.19	8.10	2.00	−0.14	2.89	Subunit IA	Pleistocene
7R-1, 20-22	65	3.90	26.73	69.37	8.08	1.71	−0.65	3.82		Pliocene
7R-1, 38-40	63	5.94	24.24	69.81	8.58	1.93	−1.01	4.17		Pliocene
7R-2, 18-20	11	2.61	44.15	53.20	8.08	1.97	0.02	2.87		Pliocene
12R-2, 144-146	30	1.60	18.19	80.21	8.93	1.64	−0.37	3.92	Subunit IC: nannofossil claystone, claystone, nannofossil ooze	late Miocene
12R-3, 110-112	36	2.47	24.75	72.78	8.79	1.87	−0.55	3.43		late Miocene
12R-4, 8-10	61	0.01	24.91	75.09	8.86	1.35	0.38	2.77		late Miocene

Table 1 (continued).

Core, section, interval (cm)	$CaCO_3$ (%)	Sand (%)	Silt (%)	Clay (%)	Mean grain size (ø)	Deviation (ø)	Skewness (ø)	Kurtosis (ø)	Lithostratigraphic unit	Age
16R-2, 63-65	28	2.22	42.40	55.38	8.07	1.90	–0.18	2.52		middle/late Miocene
17R-2, 71-73	11	9.21	35.93	54.86	7.95	2.33	–0.52	2.53		middle/late Miocene
17R-2, 83-85	38	1.31	30.43	68.26	8.37	1.88	–0.20	2.72		middle/late Miocene
17R-2, 95-97	48	3.85	33.44	62.71	8.11	1.89	–0.45	3.13		middle/late Miocene
20R-5, 17-19	11	2.01	46.37	51.63	7.89	1.84	0.02	2.43		late Miocene
20R-5, 28-30	13	1.31	43.94	54.75	8.09	2.00	0.28	2.34		late Miocene
21R-1, 54-56	15	27.36	48.30	24.34	5.92	2.27	0.76	2.36	Subunit IIA: nannofossil claystone, nannofossil chalk	early/middle Miocene
21R-4, 83-85	40	0.21	31.58	68.21	8.71	1.69	0.06	2.62		early Miocene
22R-3, 131-133	30	2.61	29.36	68.02	8.40	1.71	–0.49	3.41		early Miocene
22R-3, 140-142	40	25.49	51.05	23.46	6.17	2.22	0.44	2.15		early Miocene
24R-2, 143-145	36	6.61	40.80	52.60	7.79	2.06	–0.17	2.48		early Miocene
25R-4, 15-17	50	12.79	47.20	40.01	7.06	2.12	0.00	2.18		early Miocene
26R-3, 16-18	31	13.16	46.69	40.14	7.14	2.31	0.05	2.05	Subunit IIB: silty claystone to clayey siltstone, nannofossil claystone, claystone	early Miocene
30R-3, 33-35	5	2.10	59.44	38.45	7.49	1.63	–0.05	3.12		early Miocene
30R-3, 49-51	13	11.33	53.14	35.52	7.04	2.20	0.23	2.38		early Miocene
32R-2, 21-23	34	2.02	46.99	51.00	8.05	1.97	–0.06	2.81		early Miocene
33R-5, 107-109	20	8.33	52.63	39.05	7.32	2.19	0.21	2.58		early Miocene
35R-2, 117-119	22	2.64	51.57	45.79	7.67	1.78	0.14	2.45		early Miocene

Note: Lithostratigraphic units from Shipboard Scientific Party (1994).

ward finding environment-diagnostic parameters/descriptors of the grain-size distribution (McLaren, 1981). Textural parameters for this study are interpreted as measuring different aspects of transport mechanisms, depositional environments, and the energy responsible for deposition (Blatt et al., 1980; Forrest and Clark, 1989).

According to the terminology of fine-grained sedimentary facies in deep water (Stow and Piper, 1984), three main sedimentary facies make up the Cenozoic section present in lithostratigraphic Units I and II at Sites 897, 898, 899, and 900: (1) pelagic and hemipelagic, (2) turbidite, and (3) contourite (Figs. 4-8). Our data confirm that during Cenozoic time, the main sedimentary processes in the Iberia Abyssal Plain consisted of a combination of differential pelagic settling, turbidity currents, and bottom currents, as stated by the Leg 149 Shipboard Scientific Party (1994).

Description of Major Sedimentary Facies Types

Pelagic and Hemipelagic Facies

The pelagic and hemipelagic facies are present throughout all Cenozoic sections recovered at Sites 897, 898, 899, and 900. Pelagic sediments are defined as "deep-sea sediments without terrigenous material," and hemipelagic sediments are defined as "deep-sea sediments containing a small amount of terrigenous material as well as remains of pelagic organisms" (Bates and Jackson, 1987).Carbonate-rich pelagic facies are represented by calcareous biogenic sediments, composed predominantly of clay-size material (65%-82%). These pelagic facies are poorly sorted (1.32 ϕ-1.93 ϕ) muds with a bimodal distribution at 9 ϕ and a small peak at 3 ϕ (Fig. 4). The median grain size varies from 7.5 ϕ to 8.7 ϕ, with a relatively low sand fraction percentage (3%-7%). Light-colored beds of clayey nannofossil ooze have a unimodal grain-size distribution at 8.5 ϕ and contain up to 80% clay-size grains. The cumulative curve of the fine-grained fraction is hyperbolic and logarithmic tending toward hyperbolic (Fig. 8). The carbonate content is normally high (65%-82%), except a few samples with a relatively low content (50%-58%). The sand fraction is composed mostly of well-preserved planktonic foraminifers.

Hemipelagic facies are characterized by a poorly sorted (1.63 ϕ-2.77 ϕ) mud with a bimodal distribution at 7.5 ϕ-8 ϕ and a small peak at 3 ϕ (Fig. 4). The median grain size varies from 7.8 ϕ to 8.7 ϕ with a low (0.20%-6.40%) sand fraction content. The cumulative curve of the fine-grained fraction is hyperbolic and logarithmic tending toward hyperbolic (Fig. 8). The sand fraction is composed largely of well- and moderately preserved planktonic foraminifers, with a trace (<1%) of terrigenous components. The sand fraction of some samples (e.g., Samples 149-899A-15R-5, 54-57 cm, 149-899A-16R-2, 15-18 cm, 149-900A-5R-5, 35-37 cm, 149-900A-21R-4, 83-85 cm, and 149-900A-24R-2, 143-145 cm) is also formed by siliceous biogenic components (radiolarians, diatoms, and silicoflagellates). The carbonate content varies from <5% to 49%. The minimum values of the carbonate content correspond to samples formed by a high percentage of siliceous components.

Turbidite Facies

The turbidite facies include sediments with three different types of texture: sand, silt, and clay. We identified the Ta, Tb, Tc, Td, and Te divisions described for the Bouma (1962) turbidite sequences. The Ta and Tb divisions were recovered only at Sites 897 and 898. The Tc division was identified at Sites 897, 898, and 899. The Td and Te divisions were identified at all sites (897, 898, 899, and 900). The sand fraction of these sediments consists of terrigenous and terrigenous-biogenic deposits.

The Ta division shows two types of textures: coarse sand (<1.5 ϕ) and fine sand (>1.5 ϕ). The standard deviation (0.6 ϕ) is better in coarse sands than in fine-grained sands (from 1.4 ϕ to 1.8 ϕ). The size distributions are positively skewed. The coarse sands have a mean grain size at 1 ϕ-1.5 ϕ and fine sands at 3 ϕ (Fig. 5). Settling curves for Ta fine-grained divisions are parabolic (Fig. 8). The carbonate content (6%-8%) is the lowest obtained for the turbidite facies. The sand fraction is composed mainly of terrigenous components (98%): mainly light minerals (70%), mica (3%), and pyrite (<3%). Some samples (e.g., 149-898A-5H-3, 59-61 cm, and 149-898A-10H-6, 95-97 cm) contain abundant mica (22%). Unidentified shell fragments are present in relatively significant percentages (40%) in some samples (e.g., 149-897A-1R-1, 25-27 cm).

The Tb division corresponds to a silty sand texture. On the basis of standard deviation, two different subtypes were identified: poorly sorted (1.50 ϕ) and very poorly sorted (2.60 ϕ) silty sands. The silty sands have a median grain size of 5 ϕ, a skewness close to zero, and a mode at 3 ϕ. The fine-grained settling curves have long tails toward the finest fractions (Fig. 5). The cumulative curve of the pelitic fraction is logarithmic with a parabolic tendency (Fig. 8). The carbonate content is low (8%-17%), and the sand fraction is composed of terrigenous components (88%-97%) that are mainly light minerals, pyrite, and mica.

The Tc division corresponds to very poorly sorted (2.80 ϕ) silty sands and sandy silts with a median grain size of 5.0 ϕ to 6.3 ϕ. These divisions have a mode at 3 ϕ with long tails toward the fine-grained

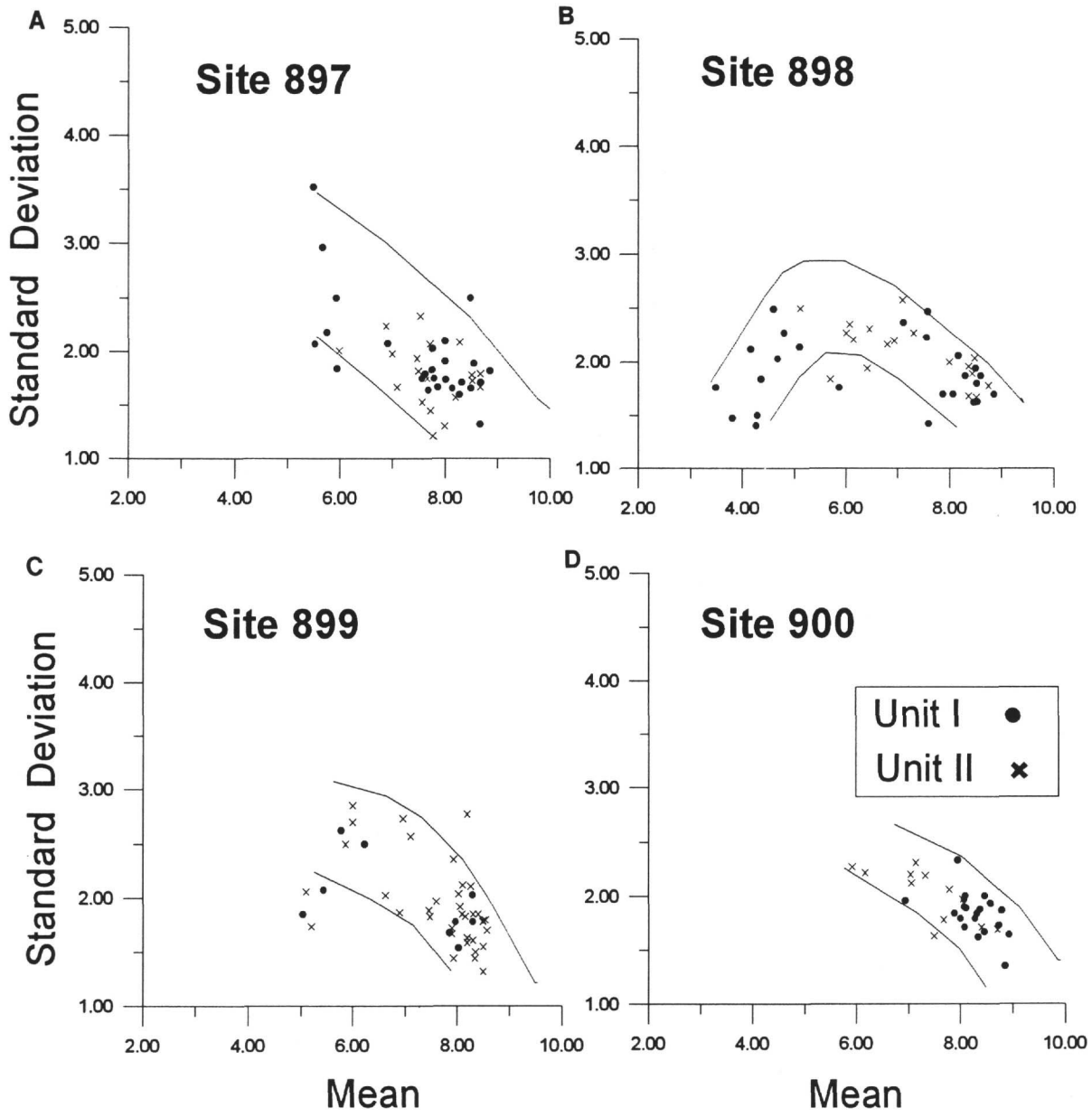

Figure 2. Binary plots of standard deviation vs. mean grain size (ϕ) for samples from Units I and II (Sites 897, 898, 899, and 900) in the Iberia Abyssal Plain.

fractions (Fig. 5). The cumulative curve of the pelitic fraction is logarithmic with a parabolic tendency (Fig. 8). The skewness varies from 0.2 to 1.0. The carbonate content is low (8%-24%). The sand fraction is composed of terrigenous (40%-100%) and biogenic components (0%-60%). Mica percentages are relatively high (31%) in some samples (e.g., 149-898A-12H-4, 32-34 cm).

The Td division corresponds to poorly sorted (1.6-2.0 ϕ) silt and muddy silt textures characterized by a median grain size of 7.0 ϕ and by a skewness close to zero. These divisions have a mode at 5.5 ϕ-6 ϕ (Fig. 5). The cumulative curve of the pelitic fraction is logarithmic tending toward parabolic (Fig. 8). The skewness values are positive close to zero. The carbonate content ranges from 6% to 40%. The sand fraction is composed of terrigenous (40%-98%) and biogenic components (2%-60%), mainly light minerals and planktonic foraminifers, respectively, and also includes traces (<5%) of mica, pyrite, and benthic foraminifers. Mica percentages are higher (58%) in some samples (e.g., 149-897A-1R-1, 63-65 cm).

Within the Te division, we identified the Te1, Te2, and Te3 divisions corresponding to Piper's (1978) sequence for fine-grained turbidite deposits. The Te division is composed of terrigenous (40%-99%) and biogenic components (1%-60%), with large amounts of light minerals and planktonic foraminifers. In general, mica, pyrite, and benthic foraminifers are present in trace amounts, but mica percentages are relatively high (57%) in some samples (e.g., 149-897C-49R-4, 13-15 cm).

The Te1 division is represented by poorly sorted (1.5 ϕ to 2.1 ϕ) muds and is characterized by a median grain size of 7.7 ϕ with a positive skewness generally close to zero. These sediments have a mode at 7 ϕ-8 ϕ (Fig. 6). The cumulative curve of the fine-grained fraction is logarithmic (Fig. 8). The total carbonate content varies from 4% to 42%.

The Te2 division is represented by poorly sorted (1.80 ϕ) muds with a median grain size up to 8.0 ϕ and a mode at 7 ϕ-8 ϕ (Fig. 6). The cumulative curve is logarithmic (Fig. 8). The carbonate content is variable, ranging from 3% to 33%.

The Te3 division is represented by poorly sorted (1.4 ϕ-2.0 ϕ) muds with high values of median grain size (8 ϕ to 9 ϕ). These sediments have a mode at 9 ϕ, with long tails on the settling curve toward

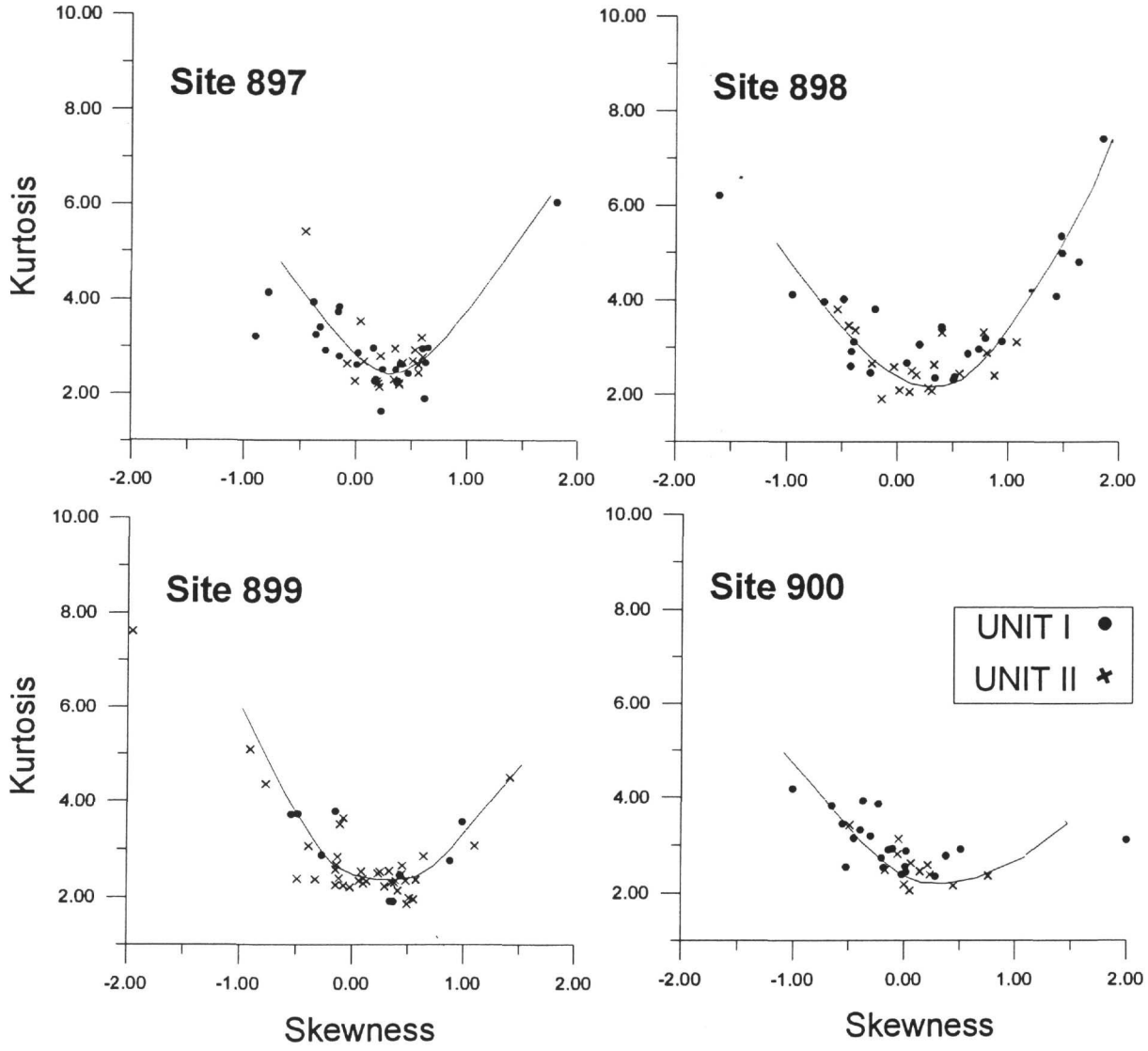

Figure 3. Binary plots of kurtosis vs. skewness for samples from Units I and II (Sites 897, 988, 899, and 900) in the Iberia Abyssal Plain.

the fine-grained fractions (Fig. 6). The skewness is positive and negative close to zero. The cumulative curve of the fine-grained fraction is logarithmic (Fig. 8). The carbonate content ranges from 4% to 60%.

Contourite Facies

Separating turbidites from contourites has always been problematic, especially when bottom currents modify deposits containing turbidites (Faugères and Stow, 1993). In the Iberia Abyssal Plain, in addition to evidence for turbidity currents and pelagic settling, some evidence for occasional bottom-current activity exists in spite of the difficulty distinguishing lithologic features of modern and fossil contourites from turbidites.

This evidence is found in some sandy layers with a low pelite content (<19%-30%) that contain high concentrations (up to 90%) of coarse foraminiferal test remains. These layers were identified at Site 897 within Unit II (Sample 149-897C-30R-4, 40-42 cm), at Site 898 within Unit I, (Sample 149-898A-1H-5, 128-130 cm), and at Site 899 within Unit II (Sample 149-899A-14R-3, 62-64 cm). Rupke and Stanley (1974) found pteropod shell layers in the Algero-Balearic Basin; Comas and Maldonado (1988) found foraminiferal sands during Leg 103 in the Iberia Abyssal Plain; and Faugères et al. (1979) also described pure foraminiferal contourite sands in the North Atlantic Basin. Those authors have hypothesized that these deposits seem to be a winnowed concentration formed by normal bottom currents.

In addition to sandy sediments in the Iberia Abyssal Plain, silty sediments with mixtures of biogenous and terrigenous or only biogenous composition were recognized at all studied sites. These silty sediments were recognized in Hole 897C within Unit I (e.g., Samples 149-897C-10R-1, 88-90 cm, 16R-2, 37-39 cm, and 19R-3, 38-40 cm) and Subunit IIB (e.g., Sample 149-897C-40R-6, 71-74 cm); in Hole 898A within Subunit IIB (e.g., Samples 149-898A-19X-6, 84-86 cm, and 29X-3, 12-14 cm); in Hole 899A within Subunit I (e.g., Sample 149-899A-16X-2, 95-97 cm) and Subunit IIB (e.g., Samples 149-899A-14R-2, 108-110 cm, and 15R-5, 58-61 cm); and in Hole 900A (Samples 149-900A-21R-5, 28-30 cm, 25R-4, 15-17 cm, and 26R-3, 16-18 cm). These deposits could be attributed to the effect of bottom-current processes. The silty deposits are differentiated from the Td division turbidites on the basis of the following diagnostic features: (1) bimodal and polymodal grain-size distributions in the total cumulative curve, (2) the lack of vertical grading in terms of textures and sedimentary structures, and (3) poorly preserved nannoplankton.

Taking these data into account, we distinguished two types of contourite facies: (1) sandy contourites resulting from a combination reworking and deposition from bottom currents and (2) silty contou-

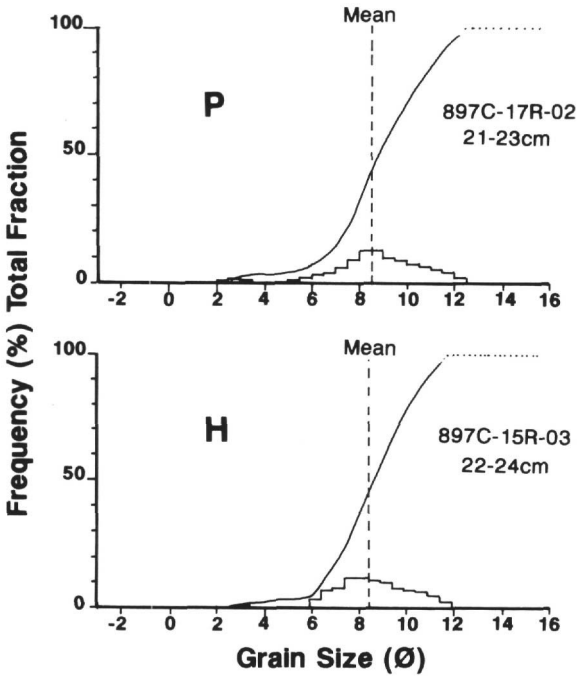

Figure 4. Textural cumulative curves and frequency histograms of representative pelagic facies (P) and representative hemipelagic facies (H) identified in the Iberia Abyssal Plain.

rites resulting from the deposition action of bottom currents, according to Stow and Piper (1984).

The sandy contourites consist of poorly sorted (1.85 ϕ-2.96 ϕ) silty sands and have a median grain size of 5 ϕ with low percentages of the clay fraction (9%) (Fig. 6). The grain-size distribution is bimodal, with a main mode at 3 ϕ-4 ϕ and a subordinate mode at 6 ϕ-8 ϕ (Fig. 7). The cumulative curve of the pelitic fraction is logarithmic tending toward parabolic (Fig. 8). The carbonate content is uniformly high (41%-48%). The sand fraction is composed largely of planktonic foraminifers.

We discriminated two subtypes of silty contourites on the basis of sand composition and carbonate content: (1) carbonate silty contourites and (2) terrigenous silty contourites. The carbonate silty contourites are characterized by poorly sorted (2.0 ϕ-2.2 ϕ) clayey silts with relatively high amounts of the sand fraction (up to 26%). The main grain size varies between 6.0 ϕ and 6.9 ϕ. The grain-size distribution is polymodal, with modes at 3.5 ϕ-4 ϕ, 5.5 ϕ-6 ϕ, and 7.5 ϕ-8.5 ϕ (Fig. 7). The cumulative curve of the pelite fraction is parabolic tending toward logarithmic, but the curve shape is convex upward between 11 ϕ and 3 ϕ, which is related to the presence of nannofossils. The carbonate content is relatively high (35%-47%). The sand fraction is formed by biogenic components (70%) represented mainly by planktonic foraminifers (66%) and siliceous biogenic clasts (15%-23%).

The terrigenous silty contourites consist of poorly sorted grains (2.0 ϕ-2.3 ϕ) with a median grain size of 5.4 ϕ to 6.8 ϕ. The grain-size distribution is bimodal, at 3.5 ϕ-4 ϕ and 5 ϕ-5.5 ϕ, with a long tail in the finer fraction (Fig. 7). The cumulative curve of the pelitic fraction is parabolic and parabolic tending toward logarithmic (Fig. 8). The carbonate content is lower (6%-23%) than in the sandy contourites. The sand fraction is dominated by terrigenous components (80%), especially light minerals and mica.

Bulk Mineralogy

Bulk mineralogy was determined for 28 samples chosen as representative of the sedimentary facies described for the Iberia Abyssal

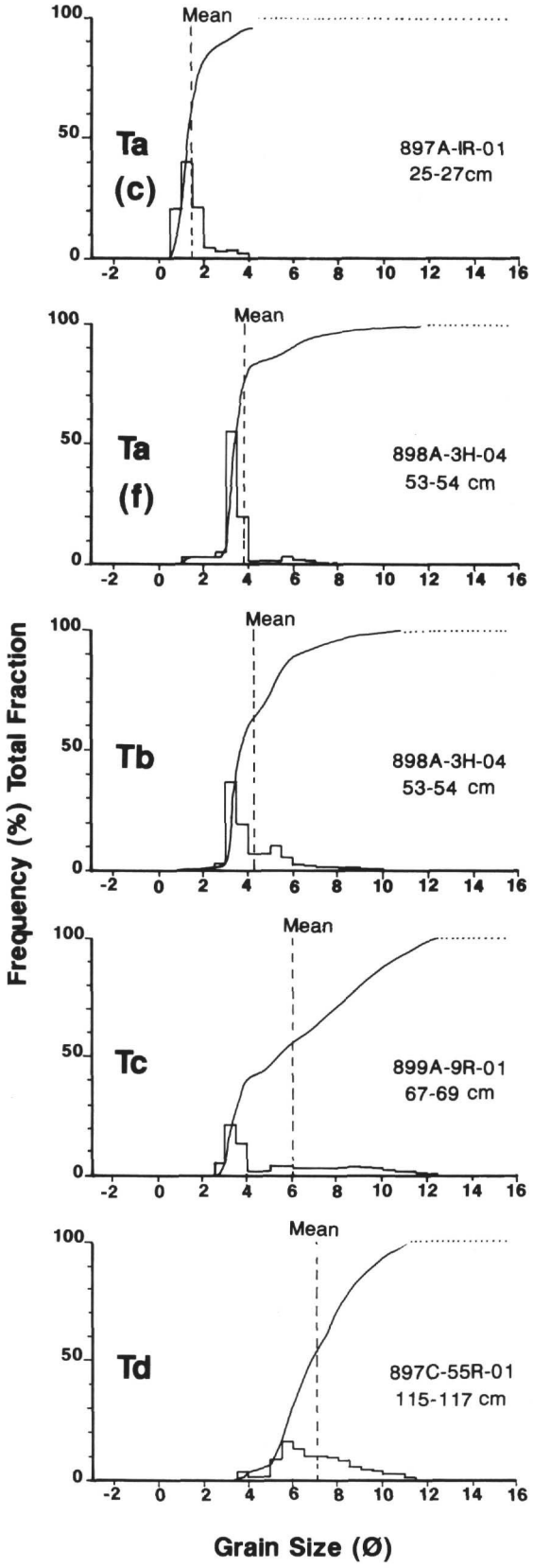

Figure 5. Textural cumulative curves and frequency histograms of silt and sand turbidite facies identified in the Iberia Abyssal Plain. The Ta, Tb, Tc, and Td divisions refer to the turbidite sequence described by Bouma (1962); c = coarse grained; f = fine grained.

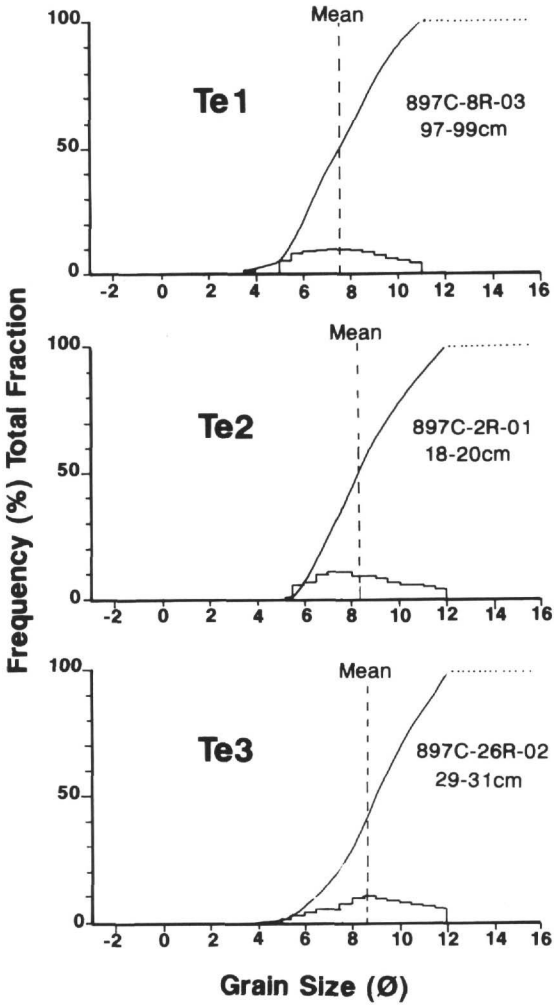

Figure 6. Textural cumulative curves and frequency histograms of mud turbidite facies identified in the Iberia Abyssal Plain. The Te1, Te2, and Te3 divisions correspond to Piper's (1978) sequence of fine-grained turbidite deposits.

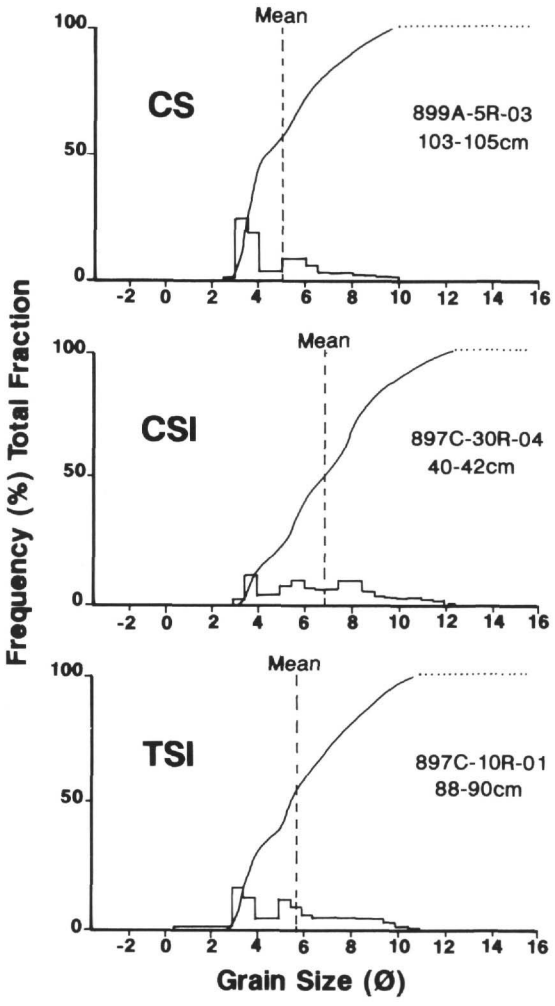

Figure 7. Textural cumulative curves and frequency histograms of contourite facies identified in the Iberia Abyssal Plain. CS = sandy contourites; CSI = calcareous silty contourites, TSI = terrigenous silty contourites.

Plain. The relative percentages of the major crystalline components (illite, kaolinite, chlorite, quartz, calcite, dolomite, feldspar, and plagioclase) of sediments from Sites 897, 898, 899, and 900 are presented in Table 2. The major sedimentary facies, which were identified on basis of textural results, are also characterized by significant differences in the bulk mineralogy (Fig. 9).

The bulk mineralogy of the pelagic facies reveals a high calcite contents (53%-76%) with a low abundance of clay minerals (illite 11%-19%, kaolinite 0%-6%, chlorite 0%-8%) and quartz (8%-12%) and very low feldspar (0%-11%) and plagioclase (0%-4%) (Table 2, Fig. 9).

The bulk mineralogy of the hemipelagic facies shows variable quartz (15%-51 %) and calcite (10%-39%) contents, with a low clay-mineral content (illite 9%-23%, kaolinite 0%-8%, chlorite 0%-9%) and a low abundance of feldspar (9%-12%) and plagioclase (8%-21%) (Table 2, Fig. 9).

The turbidite facies exhibits a variable mineralogical composition. Three main types of turbidite deposits can be distinguished on the basis of their bulk mineralogical content: (1) turbidite sand and silt with a variable quartz content (32%-65%), which is inversely related to calcite content (4%-34%), low clay-mineral content (illite 6%-12%, chlorite and kaolinite 0%), and low amounts of feldspar (9%-12%) and plagioclase (11%-21%); (2) turbidite mud containing abundant amounts of clay minerals (illite 25%-36%, chlorite 23%-25%, kaolinite 11%-18%), with a relatively high quartz content (23%-25%) and very low to absent calcite content (0%-7%); and (3) turbidite mud that has higher calcite content (31%-46%) and lower clay-mineral (illite 14%-36%, chlorite 0%-17%, kaolinite 0%-13%) and quartz (15%-20%) contents than the type 2 turbidite facies (Table 2, Fig. 9).

The bulk mineralogy of the contourite facies shows relatively high contents of calcite (30%-47%), quartz (15%-42%), feldspar (10%), and plagioclase (10%-21%) and low contents of clay minerals (illite 6%-16%, chlorite 0%, kaolinite 0%). Sandy contourites have higher quartz and lower illite percentages than silty contourites (Table 2, Fig. 9).

SUMMARY

The textural analysis, sand fraction composition, carbonate content, and bulk mineralogy provide adequate data to typify the sedimentary facies of the Cenozoic sediment cores recovered from ODP Sites 897, 898, 899, and 900 on the Iberia Abyssal Plain. According

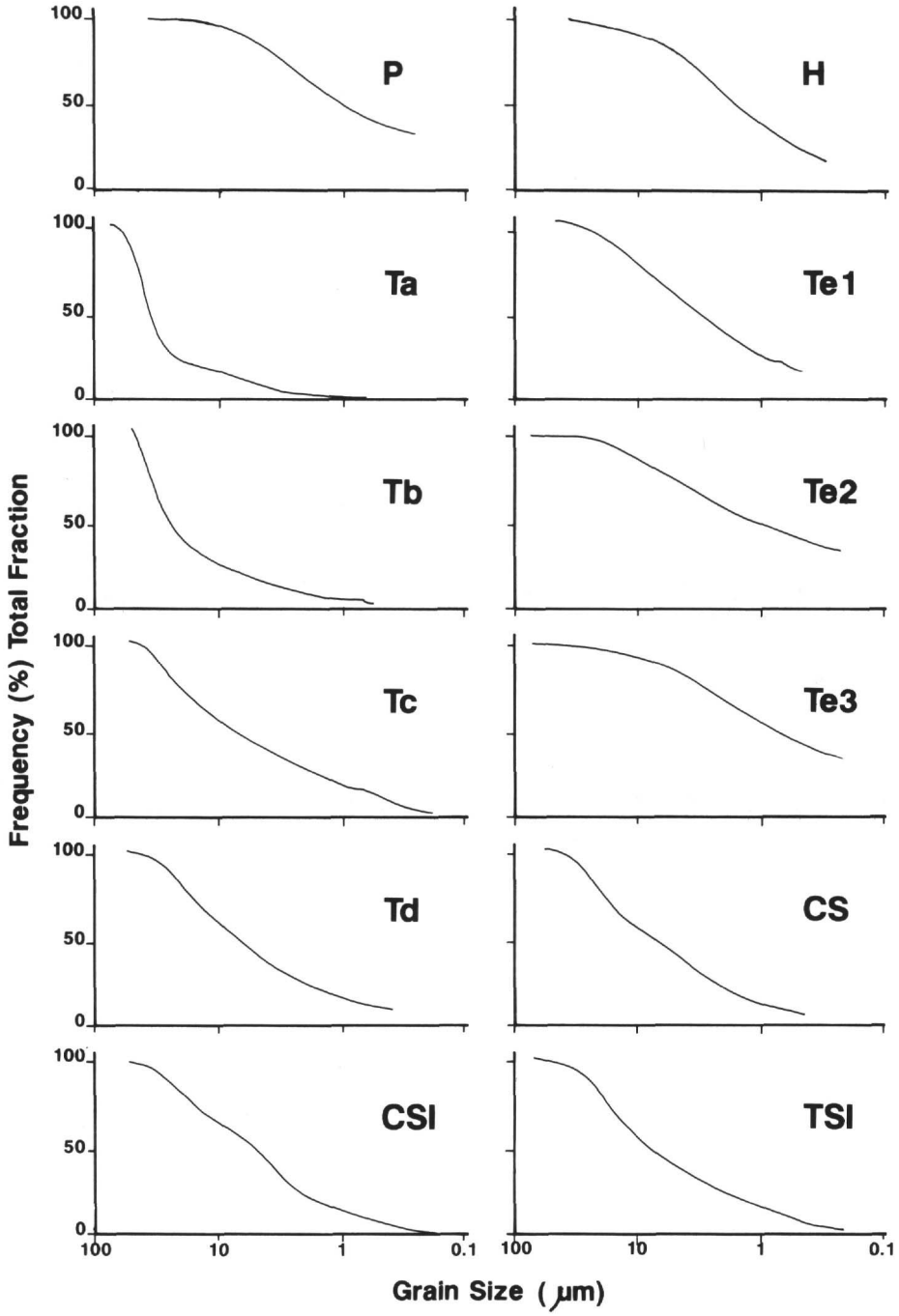

Figure 8. Representative cumulative curves of the fine-grained fraction (<50 μm) of different sedimentary facies identified in the Iberia Abyssal Plain. P = pelagic (Sample 149-897C-17R-2, 21-23 cm); Ta division (Sample 149-898A-8H-2, 120-122 cm); Tb division (Sample 149-898A-3H-4, 53-55 cm); Tc division (Sample 149-899A-1R-3, 68-70 cm); Td division (Sample 149-987C-50R-1, 143-145 cm); CSI = carbonate silty contourites (Sample 149-898A-19X-CC, 18-20 cm); H = hemipelagic (Sample 149-897C-15R-3, 22-24 cm); Te1 turbidite mud (Sample 149-897C-8R-3, 97-99 cm); Te2 turbidite mud (Sample 149-897C-2R-1, 65-67 cm); Te3 turbidite mud (Sample 149-900A-6R-6, 90-92 cm); CS = sandy contourites (Sample 149-898A-1H-5, 128-130 cm); and TSI = terrigenous silty contourites (Sample 149-898A-30X-3, 131-133 cm).

to this data, the Cenozoic sedimentary facies at these sites include pelagic/hemipelagic deposits, turbidite deposits, and contourite deposits, as indicated by Leg 149 Shipboard Scientific Party (1994).

Similar sedimentary facies were described and textural analysis data were taken into account in other areas close to Iberia Abyssal Plain, such as the distal North Atlantic continental margin off Portugal (Deep Sea Drilling Project [DSDP] Leg 47; Maldonado, 1979) and the Galicia Margin (ODP Leg 103; Comas and Maldonado, 1988). The textural data presented in this report can be used for sedimentological purposes and for understanding the sedimentary processes on the Iberia Abyssal Plain (Milkert et al., chapter 45, this volume).

ACKNOWLEDGMENTS

We thank S. O'Connell and A. Klaus for corrections and comments. We greatly appreciate the assistance of the scientific party and crew of the *JOIDES Resolution* in the acquisition of these data. We thank N. Maestro and B. Paracuellos for their help in the laboratory. J.M. Anguita drew the final figures. This work was supported through the "DGICYT" of Spain under grant PB91-0080-C02-02.

REFERENCES

Alonso, B., and Maldonado, A., 1990. Late Quaternary sedimentation of the Ebro turbidite systems (Northwestern Mediterranean): two styles of deep-sea deposition. *Mar. Geol.,* 95:353-377.

Bates, R.L., and Jackson, J.A. (Eds.), 1987. *Glossary of Geology* (3rd ed.): Alexandria, VA (Am. Geol. Inst.).

Blatt, H., Middleton, G., and Murray, R., 1980. *Origin of Sedimentary Rocks* (2nd ed.): Englewood Cliffs, NJ (Prentice-Hall).

Bouma, A.H., 1962. *Sedimentology of Some Flysch Deposits: A Graphic Approach to Facies Interpretation:* Amsterdam (Elsevier).

Comas, M.C., and Maldonado, A., 1988. Late Cenozoic sedimentary facies and processes in the Iberian Abyssal Plain, Site 637, ODP Leg 103. *In* Boillot, G., Winterer, E.L., et al., *Proc. ODP, Sci. Results,* 103: College Station, TX (Ocean Drilling Program), 635-655.

Ercilla, G., Alonso, B., and Baraza, J., 1994. Post-Calabrian sequence stratigraphy of the northwestern Alboran Sea (Southwestern Mediterranean). *Mar. Geol.,* 120:249-265.

Faugères, J.C., Gayet, J., Gonthier, E., Grousset, F., Latouche, C., Maillet, N., Poutiers, J., and Tastet, J.P., 1979. Evolution de la sédimentation profunde au Quaternaire récent dans le Bassin nord-atlantique: corps sedimentaires et sédimentation ubiquiste. *Bull. Soc. Geol. Fr.,* 21:585-601.

Faugères, J.C., and Stow, A.V., 1993. Bottom-current-controlled sedimentation: a synthesis of the contourite problem. *Sediment. Geol,* 82:287-297.

Forrest, J., and Clark, N.R., 1989. Characterizing grain size distributions: evaluation of a new approach using a multivariate extension of entropy analysis. *Sedimentology,* 36:711-722.

Friedman, G.M., and Sanders, J., 1978. *Principles of Sedimentology:* New York (Wiley), 58-81.

Giró, S., and Maldonado, A., 1985. Análisis granulométrico por métodos automáticos: tubo de sedimentación y Sedigraph. *Acta Geol. Hisp.,* 20:95-102.

Gonthier, E., Faugères, J.C., and Weber, O., 1981. Signification des méthodes granulométriques pour la reconstitution des processus hydrodynamiques à partir de sédiments terrigènes carbonatés de milieux marins profonds. *Bull. Inst. Geol. Bassin Aquitaine,* 30:31-49.

Maldonado, A., 1979. Upper Cretaceous and Cenozoic depositional processes and facies in the distal North Atlantic continental margin off Portugal, DSDP Site 398. *In* Sibuet, J.-C., Ryan, W.B.F., et al., *Init. Repts. DSDP,* 47 (Pt. 2): Washington (U.S. Govt. Printing Office), 373-402.

McLaren, P., 1981. An interpretation of trends in grain size measures. *J. Sediment. Petrol.,* 51:611-624.

Palanques, A., and Maldonado, A., 1985. Sedimentología y evolución del Valle-Abanico de Valencia (Mediterráneo Noroccidental). *Acta Geol. Hisp.,* 20:1-19.

Palanques, A., Plana, F., and Maldonado, A., 1990. Recent influence of man on the Ebro margin sedimentation system, northwestern Mediterranean Sea. *Mar. Geol.,* 95:247-263.

Piper, D.J.W., 1978. Turbidite muds and silts on deepsea fans and abyssal plains. *In* Stanley, D.J., and Kelling, G. (Eds.), *Sedimentation in Submarine Canyons, Fans and Trenches:* Stroudsburg, PA (Dowden, Hutchinson and Ross), 163-175.

Rius, J., Plana, F., and Palanques, A., 1989. A standardless X-ray diffraction method for the quantitative analysis of multiphase mixtures. *J. Appl. Crystallogr.,* 20:457-460.

Riviere, A., 1977. *Méthodes Granulometrics: Techniques et Interpretations:* Paris (Masson).

Rupke, N.A., and Stanley, D.J., 1974. Distinctive properties of turbiditic and hemipelagic mud layers in the Algero-Balearic Basin Western Mediterranean Sea. *Contrib. Earth Sci.,* 13:1-40.

Sawyer, D.S., Whitmarsh, R.B., Klaus, A., et al., 1994. *Proc. ODP, Init. Repts.,* 149: College Station, TX (Ocean Drilling Program).

Sly, P.G., Thomas, R.L., and Pelletier, B.R., 1983. Interpretation of moment measures derived from water-lain sediments. *Sedimentology,* 30:219-233.

Stow, D.A.V., and Piper, D.J.W., 1984. Deep-water fine-grained sediments: facies models. *In* Stow, D.A.V., and Piper, D.J.W. (Eds.), *Fine-grained Sediments: Deep-Water Processes and Facies.* Geol. Soc. Spec. Publ. London, 15:611-645.

Vatan, A., 1967. *Manuel de Sédimentologie:* Paris (Technip.).

Date of initial receipt: 5 December 1994
Date of acceptance: 22 May 1995
Ms 149SR-252

Table 2. Bulk mineralogy data from recovered Cenozoic sediments (Holes 897C, 898A, 899A, and 900A).

Core, section, interval (cm)	Facies	Illite (%)	Kaolinite (%)	Chlorite (%)	Quartz (%)	Calcite (%)	Dolomite (%)	Feldspar (%)	Plagioclase (%)	Lithostratigraphic unit	Age
149-897C-											
5R-1, 85-87	Te3	14	0	17	22	46	0	0	0	Unit I	Pleistocene
14R-2, 32-34	Te1	31	8	14	16	16	5	5	5	Unit I	Pliocene
17R-2, 21-23	P	14	0	0	9	76	0	0	0	Unit I	Pliocene
3R-4, 40-42	CS	10	0	0	17	47	3	10	13	Subunit IIB	Miocene
49R-3, 49-51	Te3	36	11	13	23	0	0	7	11	Subunit IIC	Oligocene
49R-2, 130-132	Te1	22	0	0	19	34	2	9	13	Subunit IIC	Oligocene
51R-2, 47-49	Te1	20	0	9	17	36	2	6	9	Subunit IIC	Eocene
149-898A-											
1H-5, 128-130	Tb	9	0	0	32	34	1	12	11	Unit I	Pleistocene
1H-5, 145-147	H	9	0	0	51	20	3	9	8	Unit I	Pleistocene
5H-6, 35-37	Te3	27	18	16	25	0	0	6	8	Unit I	Pleistocene
8H-2, 120-122	Ta	6	0	0	65	4	2	9	13	Unit I	Pleistocene
13H-4, 32-34	P	18	0	8	9	53	0	11	0	Unit I	Pleistocene
16X-2, 95-97	Tb	12	0	0	39	11	2	19	14	Unit I	Pleistocene
18X-4, 97-100	Te3	17	0	0	54	7	0	9	12	Unit I	Pliocene
19X-CC, 18-20	CSI	16	0	0	15	35	2	10	21	Subunit IIB	Miocene
22X-1, 130-132	CSI	14	0	0	25	39	0	9	14	Subunit IIB	Miocene
149-899A-											
4R-1, 43-45	P	19	6	7	9	55	0	2	3	Unit I	Pliocene
4R-2, 28-30	Te1	25	14	15	23	7	1	7	8	Unit I	Pliocene
5R-3, 100-102	P	11	4	4	8	68	0	2	4	Unit I	Pliocene
6R-2, 100-102	CSI	6	0	0	42	30	2	10	10	Subunit IIA	Miocene
14R-3, 62-64	CS	6	0	0	24	40	1	10	18	Subunit IIB	Miocene
15R-5, 54-57	H	23	8	9	18	26	2	7	7	Subunit IIB	Miocene
149-900A-											
6R-6, 80-82	P	15	0	0	12	72	0	0	0	Subunit IA	Pleistocene
12R-2, 144-146	Te3	19	13	0	17	43	0	0	8	Subunit IC	late Miocene
17R-2, 83-85	Te3	26	0	10	15	31	2	9	6	Subunit IC	middle Miocene
21R-1, 54-56	TSI	10	0	0	41	15	3	9	21	Subunit IIA	early Miocene
24R-2, 143-145	H	20	0	7	15	32	2	12	13	Subunit IIA	early Miocene
30R-3, 49-51	H	21	0	8	31	10	3	9	18	Subunit IIB	early Miocene

Notes: Facies types: P = pelagic; H = hemipelagic; CS = sandy contourites; CSI = carbonate silty contourites; Ta, Tb = turbidite divisions; Te1, Te2, Te3 = turbidite muds. Lithostratigraphic units from Shipboard Scientific Party (1994).

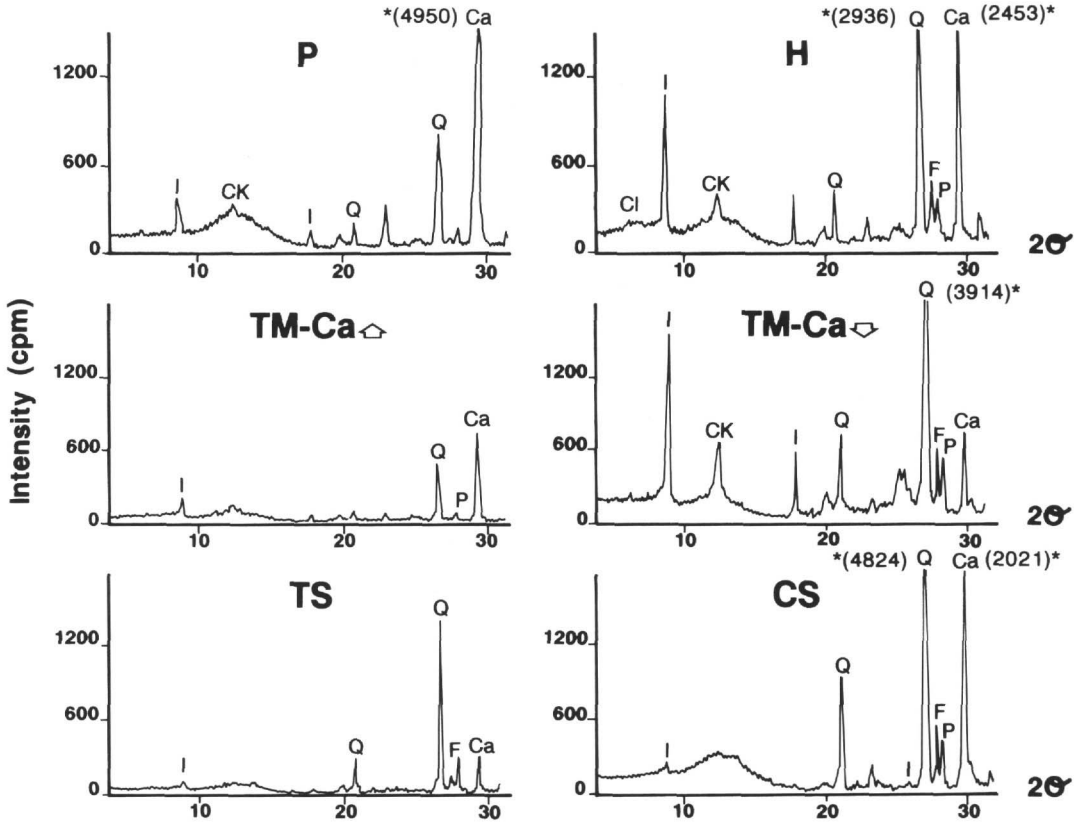

Figure 9. Representative X-ray-diffraction patterns of the total fraction from samples corresponding to the pelagic facies (P: Sample 149-899A-5R-3, 100-103 cm), hemipelagic facies (H: Sample 149-899A-15R-5, 54-57 cm), turbidite mud with high calcite content (TM-Ca↑: Sample 149-900A-12R-2, 144-146 cm), turbidite mud with low calcite content (TM-Ca↓: Sample 149-899A-4R-2, 28-30 cm), turbidite sands (TS: Sample 149-900A-21R-1, 54-56 cm), and sandy contourite sediments (CS: Sample 149-899A-6R-2, 100-102 cm). Values off the vertical scale are in parentheses and marked with an asterisk.

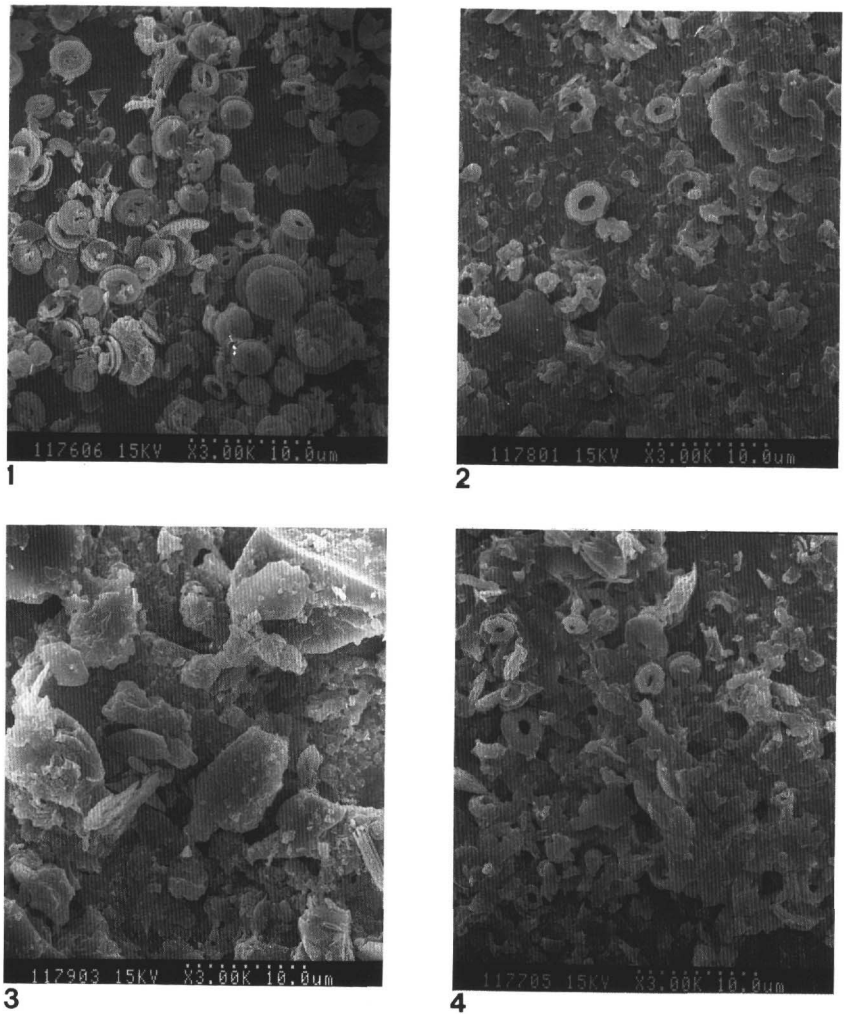

Plate 1. SEM photomicrographs of the silt- and clay-size fraction from pelagic, hemipelagic, turbidite, and contourite facies. **1.** Pleistocene biogenic pelagic facies with abundant and well-preserved nannofossils (Sample 149-898A-3H-4, 7-9 cm). **2.** Upper Pliocene hemipelagic facies with clay and well- to moderately preserved nannofossils (Sample 149-898A-18X-6, 129-130 cm). **3.** Uppermost Pliocene mud turbidite with a notable absence of nannofossils (Sample 149-898A-5H-5, 59-61 cm). **4.** Upper Oligocene carbonate silty contourite with moderately to poorly preserved nannofossils (Sample 149-898A-33X-2, 143-145 cm).